Counter-propagating Rossby waves in the barotropic Rayleigh model of shear instability

By E. HEIFETZ[1]*, C. H. BISHOP[2] and P. ALPERT[1]

[1]*Tel-Aviv University, Israel*
[2]*The Pennsylvania State University, USA*

SUMMARY

Wave development, using Rayleigh's 1880 model of barotropic, inviscid and incompressible flow, with a mean zonal wind which is linearly sheared between two edges, is described in terms of the interaction between two counter-propagating Rossby waves (CRWs). Although the solutions described by this approach could also be described by a sum of the normal modes originally obtained by Rayleigh, we offer a CRW description of Rayleigh's model because it provides a useful pedagogical framework for illustrating, in a precise and quantifiable manner, the interacting Rossby wave view of instability. A CRW interpretation of a modified version of the Rayleigh model, consisting of a jet-like flow featuring two strips of vorticity with opposite signs, is also given.

KEYWORDS: Counter-propagating Rossby waves   Normal modes   Shear instability   Vorticity strips

1. INTRODUCTION

Bretherton (1966) showed that wave development in flows that feature two distinct potential-vorticity (PV) gradients can be interpreted in terms of the interaction of two distinct Rossby waves which propagate on the two distinct PV gradients. This explanation provided an alternative explanation of Charney and Stern's (1962) finding that the two PV gradients had to be of opposite sign in order for normal-mode (NM) instability to occur. Bretherton argued that the perturbation PV field of a NM would only be able to resist the deforming effects of a shear flow[†] if there were basic state PV gradients that allowed Rossby wave propagation to offset such deforming effects. In regions where the NM's phase speed is *positive* relative to the basic state flow, the basic state PV gradient had to provide Rossby wave propagation with a similarly *positive* phase speed, and vice versa. Since the direction of Rossby wave propagation is given by the sign of the basic state PV gradient, this means that the basic state PV gradient in some part of the region where the wave propagation, relative to the flow, is positive had to be of a different sign to the PV gradient in some part of the region where the wave propagation, relative to the flow, is negative.

Bretherton described this process of deformation resistance in terms of the interaction of two Rossby waves which propagated in opposing directions on oppositely signed PV gradients. In the terminology of Hoskins *et al.* 1985 (henceforth HMR) such Rossby waves are counter-propagating (CRWs). Bretherton and HMR considered the disturbance wind field attributable to the PV pattern in each of the waves, where 'attributable to' means attributable in the sense of what HMR called 'PV inversion'. If this wind field overlaps both regions of PV gradients, then each wave can affect the other's phase speed and/or make the other grow or decay. This effect depends on the phase relation between the two waves. The phase relation required for the two waves to resist the deforming affects of the shear was found to be dependent on the intrinsic propagation speeds of the Rossby waves. Since the intrinsic propagation speed increased as the wavelength

---

[†] Note that since, by definition, the time dependence of normal modes is separable from their spatial dependence (cf. Farrell 1984), NMs always resist the deforming effects of shear flows.

increased, Bretherton was able to infer how the phase tilts of shear-resistant structures would change with wavelength. Since these phase tilts determined whether a disturbance would grow or decay, he was also able to estimate how the growth rate of shear-resistant waves would vary with wavelength. In particular, he was able to explain why Eady's (1949) model of baroclinic instability did not support amplifying strain-resistant short waves.

In the past decade, quantitative forms of the qualitative ideas of Bretherton and HMR have been used to intepret a range of instabilities. Bishop (1993a,b) showed that the qualitative ideas of Bretherton and HMR could be expressed quantitatively, and extended to interpret the non-modal growth of baroclinic waves that were unable to resist the deforming effects of a confluent–diffluent deformation field, but were able to partially resist the deforming effects of vertical shear. Bishop and Thorpe (1994) built on the work of Dritschel *et al.* (1991) to show how the CRW perspective could be used to interpret non-modal barotropic wave growth on fronts undergoing moist deformation frontogenesis. Barcilon and Bishop (1998) also used the framework to interpret the effect of barotropic shear deformation on baroclinic waves. Recently, Bishop and Heifetz (1999) used CRWs to describe the absolute instability that arises from the interaction between the discrete and the continuous spectrum in the semi-infinite Eady basic state. Heifetz (1999) discusses work in progress to develop a general algorithm to construct CRWs from NMs, in a baroclinic and/or barotropic basic state, and applies it to the Charney (1947) problem and to a full primitive-equation model with a realistic jet. To illustrate the baroclinic CRW concept in a simple context, Davies and Bishop (1994) derived the dynamical equations for the CRWs in the Eady model.

An even simpler framework is the fundamental two-dimensional (2-D) barotropic problem of linear shear instability—the Rayleigh (1880) problem. Extensive efforts have been put into finding the eigenvalue solutions of a whole set of problems which are related to the Rayleigh problem (comprising different mean wind profiles and/or different boundary conditions), cf. the review paper by Drazin and Howard (1966). Also, Rayleigh's initial-value problem has been solved by Eliassen *et al.* (1953) and Case (1960a,b) using the Fourier–Laplace transforms analysis or, alternatively, by looking on the spatial modes evolution, Gaster (1962) and Watson (1962). More recent work on the optimal excitation of perturbations and their transient growth in a barotropic shear flow has been carried out by Farrell, e.g. Farrell (1988). The nonlinear aspects of the perturbation growth in the Rayleigh problem have been examined by Dritschel (1989). Here (in section 2), we use the Rayleigh problem only in order to demonstrate the CRW's dynamics, and its relationship to NMs, in their clearest and simplest form.

By considering the instability of a barotropic jet flow defined by two contiguous strips of vorticity with opposite signs, we illustrate how the CRW concept can be extended to flows where there are more than two important PV gradients. In section 3, we deduce the NMs of this jet flow directly from the interaction between its three CRWs. Concluding remarks appear in section 4.

2. INTERPRETATIONS OF THE RAYLEIGH PROBLEM

(a) The NM perspective

Consider a 2-D inviscid and incompressible flow with a mean zonal wind $\overline{U}$, which is linearly sheared between the two edges $y = \{-b, b\}$, see Fig. 1(a). This flow forms a
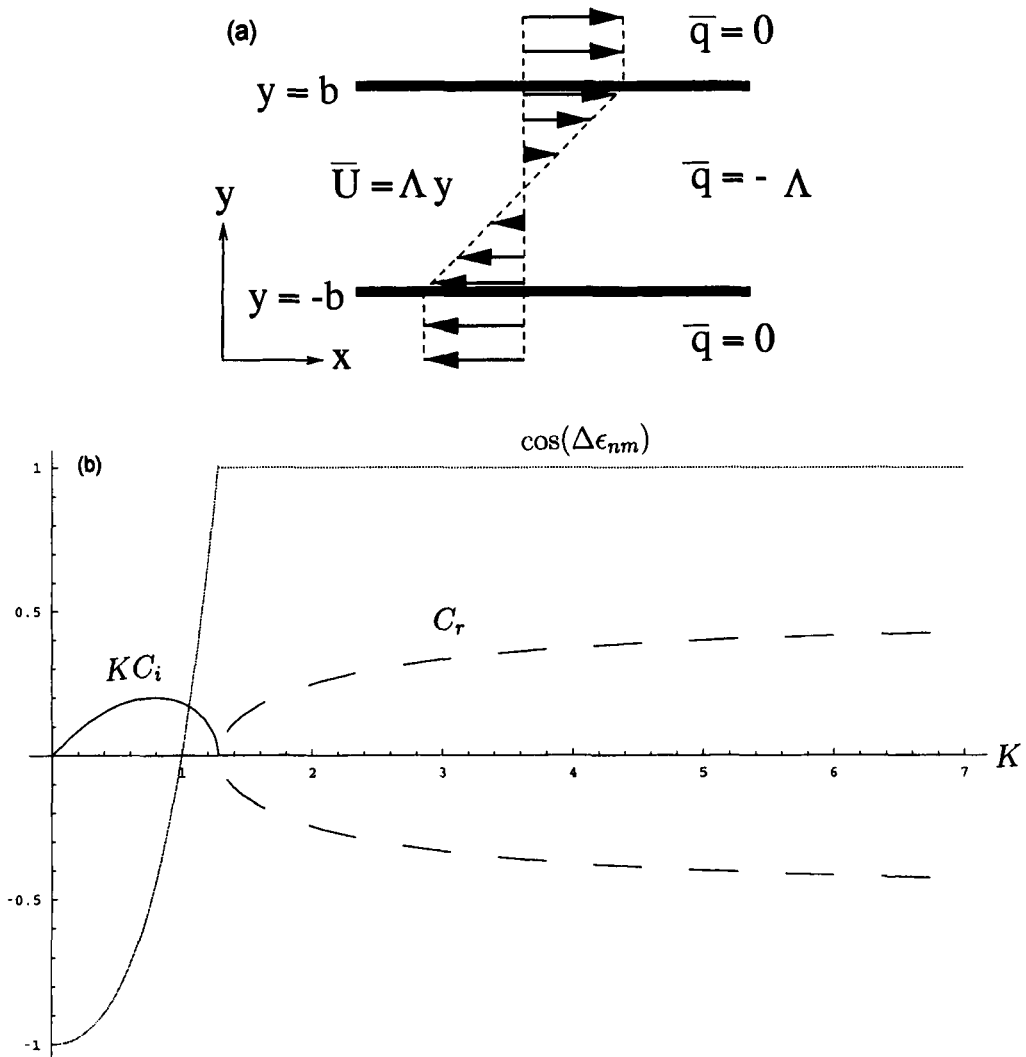
Figure 1. (a) The basic state of the classical Rayleigh model of shear instability, Eq. (1). Arrows indicate the zonal mean wind, $\overline{U}$, that forms a strip with vorticity $\overline{q} = -\Lambda$, where Λ is the shear. (b) The dispersion relation of the normal modes (NMs) in the Rayleigh model. The solid line indicates the growth rate (KC_i) normalized by Λ; the dashed line indicates the real phase speed (C_r) normalized by $2\Lambda b$, where $2b$ is the width of the shear zone. The solid grey line (discussed in section 2(b)) indicates $\cos \Delta\epsilon_{nm}$ where $\Delta\epsilon_{nm}$ is the westward phase shift of the northern counter-propagating Rossby wave (CRW) relative to the southern CRW.

strip of vorticity $\overline{q}$, equal to the negative value of the shear Λ, i.e.

$$\overline{U} = \begin{cases} \Lambda b & \text{for } y \geqslant b \\ \Lambda y & \text{for } -b < y < b \\ -\Lambda b & \text{for } y \leqslant -b \end{cases} \quad \text{and} \quad \overline{q} = \begin{cases} 0 & \text{for } y \geqslant b \\ -\Lambda & \text{for } -b < y < b \\ 0 & \text{for } y \leqslant -b \end{cases} \quad (1)$$

where y is the meridional direction in conventional cartesian (x, y) coordinates, associated with velocity components (u, v).

The NMs solution for a small disturbance, can be obtained from linearizing the vorticity equation $dq/dt = 0$ (where t is time, q is the magnitude of the vorticity vector, $\frac{\partial v}{\partial x} - \frac{\partial u}{\partial y}$, $\frac{d}{dt} = \frac{\partial}{\partial t} + \mathbf{v} \cdot \nabla$, $\mathbf{v} = (u, v) = (\overline{U} + u', v')$, and a prime indicates a

disturbance), which manifests the Lagrangian conservation of the vorticity by an air parcel. The linearization yields,

$$\left(\frac{\partial}{\partial t} + \overline{U}\frac{\partial}{\partial x}\right)q' = -v'\frac{\partial \overline{q}}{\partial y}, \tag{2}$$

where the right-hand side (r.h.s.) of (2) is zero in the interior $\{-b < y < b\}$, and singular on the edges $\{y = \pm b\}$; i.e. $-\frac{\partial \overline{q}}{\partial y} = \overline{U}_{yy} = [\overline{U}_y]_{-}^{+}\delta(y \mp b)$, where $[\overline{U}_y(y)]_{-}^{+}$ indicates the jump of the field $\overline{U}_y$ across the edges so that $[\overline{U}_y(y)]_{-}^{+} \equiv [\overline{U}_y(y+)] - [\overline{U}_y(y-)]$, where $[\overline{U}_y(y+)] = \lim_{y\downarrow\pm b}\overline{U}_y(y)$ and $[\overline{U}_y(y-)] = \lim_{y\uparrow\pm b}\overline{U}_y(y)$. Referring only to the discrete spectrum solution, then $q' = 0$ in the interior. Integrating (1) with respect to y across the edges,

$$\left(\frac{\partial}{\partial t} + \overline{U}\frac{\partial}{\partial x}\right)\int_{\pm b-\epsilon}^{\pm b+\epsilon}\left(\frac{\partial v}{\partial x} - \frac{\partial u}{\partial y}\right)\,\mathrm{d}y = (v'[\overline{U}_y]_{-}^{+})_{y=\pm b}. \tag{3}$$

Taking ϵ to zero and assuming that $\frac{\partial v}{\partial x}$ is finite everywhere, the vorticity equation on the edges can be written then as,

$$\left\{\left(\frac{\partial}{\partial t} + \overline{U}\frac{\partial}{\partial x}\right)[-u']_{-}^{+}\right\}_{y=\pm b} = (v'[\overline{U}_y]_{-}^{+})_{y=\pm b}. \tag{4}$$

Thus, defining the incompressible stream function ψ such that $(u, v) = (-\psi_y, \psi_x)$ and $q' = \nabla^2\psi'$, Rayleigh looked for NM solutions in the form of a zonal wave $\psi_{nm} = Re[\hat{\psi}(y)\,\mathrm{e}^{\mathrm{i}(kx-\omega t)}]$, with a wave number k, frequency ω and phase speed $c = \omega/k$. He wrote the meridional structure $\hat{\psi}(y)$, as

$$\hat{\psi}(y) = \begin{cases} A\,\sinh(K)\,\mathrm{e}^{-k(y-b)} & \text{for } y \geqslant b \\ A\,\sinh k(y+b) + B\,\sinh k(b-y) & \text{for } -b < y < b \\ B\,\sinh(K)\,\mathrm{e}^{k(y+b)} & \text{for } y \leqslant -b. \end{cases} \tag{5}$$

where $K = 2kb$ is the nondimensional wave number and A, B are two constant coefficients. Substituting the NMs in the boundary conditions, (4), and seeking a non-trivial solution with A, $B \neq 0$, he found the dispersion relations, Fig. 1(b),

$$C = \pm\frac{1}{2K}\{(K - 1)^2 - \mathrm{e}^{-2K}\}^{1/2}, \tag{6}$$

where $C = c/\Delta\overline{U} = c/2\Lambda b$ is the nondimensional phase speed.

Thus, for wave numbers smaller than the critical value, $K_c = 1 + \mathrm{e}^{-K_c} \approx 1.28$, the phase speeds are purely imaginary (i.e. the modes are stationary), and the NMs' growth rate, $\Lambda K C_i$, is maximum at $K_{max} \approx 0.8$, (corresponding to the wavelength $\lambda_{max} = 2\pi/K_{max} \approx$ eight times the width of the vorticity strip) and is equal to about 20% of the shear Λ, cf. Fig. 1(b). For wave numbers larger than K_c, the modes are neutral with either positive or negative real phase speeds. The amplifying and the decaying modes' amplitudes are meridionally symmetric, $|A| = |B|$, but within the strip their stream function phase lines tilt to the west with increasing latitude for the growing modes, and tilt to the east for the decaying modes. In contrast, the neutral modes' stream function phase lines do not tilt with increasing latitude and their amplitudes are meridionally asymmetric; for positive real phase speed, $|A|$ is larger than $|B|$ and vice versa for negative phase speed.

Rayleigh's standard NM analysis reveals amplifying structures which are capable of resisting the deforming affects of the shear flow. From this analysis, one can correctly predict that amplifying structures with a wavelength about 8 times the width of the shear zone will eventually emerge from any random small amplitude disturbance to the shear flow that has a non-zero projection onto the most rapidly amplifying NM. However, if we were to search this analysis for a 'reason' why and how waves grow on this shear flow, we find that 'the waves must grow because a complex phase speed is required in order that (5) and (4) be simultaneously satisfied'. The authors find this explanation rather unsatisfying. Its extreme specificity means that it gives little insight into the stability of shear flows slightly different from Rayleigh's shear flow. What would the stability of the shear flow be if the PV gradients at the edges of the vorticity strip were smooth, or if the vorticity in the region surrounding the strip were non-zero? Furthermore, the evolution of linear sums of conjugate NMs can only be inferred by evaluating their sum. One does not obtain an overview of how different initial wave structures will evolve in time. A more satisfying explanation would be one that gave such an overview, and also allowed one to make quick but qualitatively correct predictions about how the stability of the system would change as the basic state flow were changed without having to obtain the precise NM solution for each variation of the shear flow.

In our view, the missing ingredient in the normal mode 'explanation' of shear-flow instability is a pictorial story of how key features of the shear flow interact to produce wave growth. The power of explanations that translate stories or paradigms into mathematics is illustrated by Holton's (1992, p. 91), simple explanation of sea breeze development. The mathematics allows us to make quantitative predictions for a specific situation, while the pictorial story of air being heated over land more than air over the sea allows us to make qualitatively correct predictions about how sea breeze strength might vary if, for example, the albedo of the land were changed.

From Bretherton's (1966) perspective the key protagonists in stories of wave development on the Rayleigh shear flow are two Rossby edge waves, one of which propagates westward along the northern edge of the shear zone on a northward pointing PV gradient, while the other propagates eastward along the southern edge of the shear zone on a southward pointing PV gradient. The mathematical description of these entities is given in the next subsection.

(b)   The interacting Rossby wave perspective

The Rossby edge waves are the wave disturbances to the vorticity field at the edges, together with the stream function field attributable to these disturbances. The stream function field attributable to the vorticity disturbance at the northern edges is obtained by solving the Poisson equation

$$\nabla^2 \psi' = q', \tag{7}$$

subject to $\nabla \psi'$ tending to zero as $|y|$ tends to infinity, where q' is the vorticity disturbance on the northern boundary. The solution which satisfies (7) at $y = b$, with a zero q' elsewhere, can be written as:

$$\psi' = e^{-k|y-b|} e^{ikx}. \tag{8}$$

This is the inversion process relevant here. The singularity of the vorticity on b is due to the discontinuity of the perturbation zonal wind u' across the edge, so that $q' = -2k \, e^{ikx} \delta(y - b)$. Thus, in this idealized model, the Rossby wave's vorticity field is proportional to a Dirac delta function while the wind field it induces fills all space. As

such it can interact with disturbances on the southern edge. If we ignore this interaction by, for example, removing the southern edge to minus infinity, then by substituting into (2) or (4) we find that the northern wave would be advected eastwards by the westerlies while propagating westwards relative to this flow, cf. Fig. 2(a). The expression for the phase speed which results from these opposing effects is given by:

$$c_n = \overline{U}(b) + \left[\frac{\partial \overline{q}}{\partial y} \frac{\psi'}{q'} \right]_{y=b} = \overline{U}(b) \left(1 - \frac{1}{K} \right), \tag{9}$$

where the subscript n indicates the northern wave. Note that the westward Rossby propagation* is inversely proportional to the non-dimensional wave number K. When $K = 1$, the westward propagation exactly balances the eastward advection by the mean flow. For longer wavelengths, $K < 1$, westward propagation dominates eastward advection.

Similarly, the stream function field attributable to wave vorticity disturbances at the southern edge is given by:

$$\psi' = e^{-k|y+b|} e^{ikx}. \tag{10}$$

In the absence of interactions with the northern edge, the wave would propagate eastwards while being advected westwards by the mean flow. The expression for the phase speed which results from these opposing effects is given by:

$$c_s = \overline{U}(-b) \left(1 - \frac{1}{K} \right), \tag{11}$$

where the subscript s indicates the southern wave, cf. Fig. 2(b). Hence, the southern CRW is a mirror image of the northern CRW with an eastward propagation speed. Both waves propagate to the left of the local mean gradient in vorticity via the Rossby wave propagation process discussed in many textbooks, e.g. Gill (1982). The difference between the propagation rate of the northern edge wave and the southern edge wave is known as the counter-propagation rate. Note also that defining the meridional displacement η so that $v = \frac{d\eta}{dt}$, (2) can be written as:

$$\frac{dq'}{dt} = -\frac{\partial \overline{q}}{\partial y} \frac{d\eta}{dt}. \tag{12}$$

Equation (12) indicates that for perturbations, created from pure vorticity advection, the vorticity and the meridional displacement are in phase on the southern edge and 180 degrees out of phase on the northern edge; i.e. displacements away from the centre of the negative-vorticity strip always correspond to negative-vorticity anomalies, cf. Figs. 2(a) and (b).

For strips of finite width and finite wave numbers the two CRWs interact with each other through the meridional wind they induce on each other's edges. To mathematically describe this interaction we formulate our solution procedure in terms of a superposition of the two edge waves:

$$\psi' = \{ S(t) e^{-k|y+b|} e^{i\epsilon_s(t)} + N(t) e^{-k|y-b|} e^{i\epsilon_n(t)} \} e^{ikx}, \tag{13}$$

where S and N are the time dependent amplitudes of the southern and northern CRWs respectively, and ϵ_s, ϵ_n are their time dependent phases. The two degrees of freedom

---

* In order to prevent confusion: by 'Rossby propagation' we mean the propagation which is relative to the mean flow on the edge; and by 'phase speed' we mean the CRW's propagation speed relative to the stationary frame of reference.
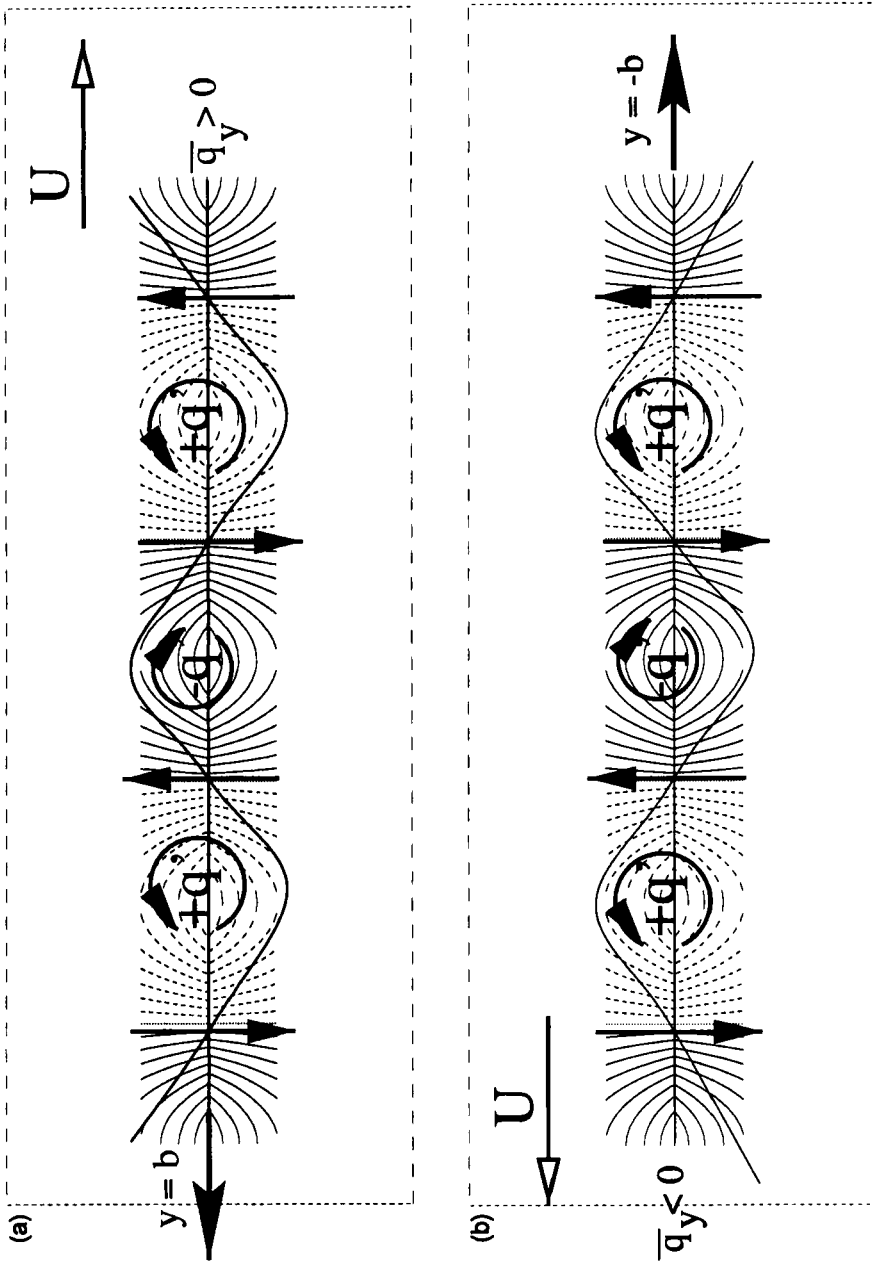
Figure 2. Schematic illustration of the counter-propagating Rossby waves (CRWs) in the Rayleigh problem: (a) and (b) represent the northern ($y = b$), and the southern ($y = -b$) CRWs, respectively. Thin solid and dashed lines indicate the positive and negative values, respectively, of the stream function attributable to each of the CRWs in the vicinity of the edges, q' is the vorticity anomaly, solid arrows indicate the CRWs meridional wind and the bold horizontal arrows indicate the CRWs counter-propagation direction. The undulating solid line illustrates the CRWs meridional displacement. The blank arrows represent the mean wind $\overline{U}$.

to initiate the system are the initial amplitude ratio $\left(\frac{N}{S}\right)_{t=0}$, and the phase difference $(\Delta\epsilon \equiv \epsilon_n - \epsilon_s)_{t=0}$. Using (13) in (4) gives the equations governing the CRWs which are:

$$\frac{1}{S}\frac{\partial S}{\partial t} = \frac{\Lambda}{2}\left\{e^{-K}\left(\frac{N}{S}\right)\right\}\sin(\Delta\epsilon), \qquad (14a)$$

$$\frac{1}{N}\frac{\partial N}{\partial t} = \frac{\Lambda}{2}\left\{e^{-K}\left(\frac{S}{N}\right)\right\}\sin(\Delta\epsilon), \qquad (14b)$$

$$c_s = -\frac{1}{k}\frac{\partial\epsilon_s}{\partial t} = \overline{U}(-b)\left[1 - \frac{1}{K}\left\{1 + \left(e^{-K}\frac{N}{S}\right)\cos(\Delta\epsilon)\right\}\right], \qquad (14c)$$

$$c_n = -\frac{1}{k}\frac{\partial\epsilon_n}{\partial t} = \overline{U}(b)\left[1 - \frac{1}{K}\left\{1 + \left(e^{-K}\frac{S}{N}\right)\cos(\Delta\epsilon)\right\}\right]. \qquad (14d)$$

This equation set is homomorphic to Eqs. (7a) to (7d) of Davies and Bishop (1994) for the temperature edge waves of the Eady model (from the CRW perspective, the Eady model is the exact analogue of the barotropic Rayleigh problem). The equations give precise descriptions of how the two Rossby waves interact with each other. To see this, consider the following.

Since the vorticity advection due to the flow attributable to the vorticity wave on the southern edge is a quarter of a wavelength out of phase with its vorticity, the southern wave cannot grow by itself; it can only make itself propagate to the left of the local mean vorticity gradient. Thus, it is only the wind field attributable to the northern vorticity wave that can affect the amplitude of the opposing southern vorticity wave.

The exact effect of the northern vorticity wave on the opposing southern vorticity wave depends on the phase difference between the two waves. If the northern wave is *less* than half a wavelength west of the southern wave, (i.e. $0 < \Delta\epsilon < \pi$), the wind attributable to the northern vorticity wave will advect positive vorticity and negative vorticity into the respective crests and troughs of the southern vorticity wave. Such increases and decreases in vorticity at the respective crests and troughs of a wave equate to wave *growth*. Conversely, if $0 > \Delta\epsilon > -\pi$ the waves attenuate. This description is in accord with (14a), which states that the growth of the southern vorticity wave is directly proportional to the product of the amplitude of the opposing northern vorticity wave (which has its attributable meridional wind attenuated on the southern edge by e^{-K}) with the sine of the westward phase displacement of the northern wave. The growth is proportional to the averaged mean vorticity on the two sides of the edge. Similarly, the southern wave affects the northern wave's growth in accordance with (14b).

If the northern wave is *less* than a quarter of a wavelength out of phase with the southern wave ($|\Delta\epsilon| < \pi/2$), the wind attributable to the northern vorticity wave reinforces the wind field attributable to the opposing southern vorticity wave. This reinforcement *increases* the rate at which the crests and troughs propagate to the left of the mean vorticity gradient. This increase in counter-propagation tends to increase the westward displacement of the northern wave. This effect is opposed by the basic state wind which would, if acting in isolation, increase the eastward displacement of the northern wave.

On the other hand, if the northern wave is *between* a quarter and a half of a wavelength out of phase with the southern wave ($\pi > |\Delta\epsilon| > \pi/2$), the wind attributable to the northern vorticity wave destructively interferes with the wind field attributable to the opposing southern vorticity wave. Such destructive interference *decreases* the rate at which the crests and troughs propagate to the left of the mean vorticity gradient. This

decrease in counter-propagation tends to decrease the westward speed of the northern wave.

These conceptual descriptions of how the two waves affect each other's propagation rates are consistent with (14c,d). These equations show that the propagation rates of the southern and northern waves to the left of the local vorticity gradient are enhanced when the cosine of $\Delta\epsilon$ is positive.

A convenient way of visualizing the complete range of structural developments described by the set (14) is to utilize a phase diagram of the type introduced by Bishop (1993a). First, note that the essential structure of the wave is uniquely defined by the inverse tangent of the amplitude ratio N/S and the phase displacement $\Delta\epsilon$. (Note that the inverse tangent of the amplitude ratio is used, because the amplitude ratio is unbounded and this is inconvenient for plotting purposes. In contrast, the inverse tangent is bounded between 0 and $\pi/2$.) Second, note that equations for the rate of change of these two parameters can be derived directly from (14), namely:

$$\dot{\gamma} = \frac{\Lambda}{2}\, e^{-K} \cos(2\gamma)\sin(\Delta\epsilon), \tag{15a}$$

$$(\dot{\Delta\epsilon}) = \Lambda \left\{ (1 - K) + \frac{e^{-K}}{\sin(2\gamma)}\cos(\Delta\epsilon) \right\}, \tag{15b}$$

where $\gamma = \arctan(N/S)$. Each γ and $\Delta\epsilon$ pair of values defines a unique structure, while (15a) and (15b) describe how this structure varies with time. Thus by plotting $(\dot{\Delta\epsilon}, \dot{\gamma})$ as vectors on the $(\Delta\epsilon, \gamma)$ plane one obtains an overview of how the $(\Delta\epsilon, \gamma)$ value of a wave of wave number K evolves in time.

Figures 3(a), (b), (c), (d) and (e) show the $(\Delta\epsilon, \gamma)$ phase diagrams for $K = 1.5$, 1.278, 1.25, 1.0, and 0.797, respectively. In interpreting these diagrams, note that at $\gamma = 0$ the northern vorticity wave has zero amplitude, and that at $\gamma = \pi/2$ the southern vorticity wave has zero amplitude. At $\gamma = \pi/4 \approx 0.785$ the two waves have equal amplitudes. Also note that according to (14a,b), the structures amplify whenever $\pi > \Delta\epsilon > 0$ and attenuate when $-\pi < \Delta\epsilon < 0$. Thus, points on the r.h.s. of the diagram correspond to growing waves, and on the l.h.s. to the decaying waves. Since it is the northern wave that makes the southern wave grow, the growth rate of the southern wave is proportional to the amplitude of the northern wave, cf. 14(b), and vice versa for the northern wave, cf. 14(a). Consequently, when $\pi > \Delta\epsilon > 0$, the smaller of the northern and southern waves grows faster. Thus, on the r.h.s. of all of the phase diagrams shown in Fig. 3, the arrows point toward the equal amplitude γ value of $\pi/4$. By similar reasoning one can show that when $-\pi < \Delta\epsilon < 0$, the smaller of the two Rossby waves decays fastest and, consequently, on the l.h.s. of all of the phase diagrams shown in Fig. 3, the arrows point away from the equal amplitude γ value of $\pi/4$.

At $K = 1.5$, we see that the $\Delta\epsilon$ values of structures which have γ values near $\pi/4$ are continuously decreasing. This is because at the relatively small wavelength corresponding to $K = 1.5$, the tendency of the shear flow to decrease $\Delta\epsilon$ cannot be offset by counter-propagation. At this wavelength, the only way the two edge waves counter-propagation rate can offset the advection by the mean flow is if there is a significant difference between the amplitudes of the upper and lower waves, cf. (15b). This is evidenced by the two spiral nodes at $(\Delta\epsilon, \gamma) = (0, 0.23); (0,1.34)$. Since the structure of NMs does not change with time, these nodes correspond to the two neutral NMs (indicated by n1 and n2 in the diagram). Note also that at $\Delta\epsilon = 0$ and $\gamma < \gamma_{\text{neutral mode 1}}; \gamma > \gamma_{\text{netural mode 2}}$ the counter-propagation exceeds mean flow advection and $\Delta\epsilon$ increases with time. Furthermore, when the amplitude of one of the waves is vanishingly small, counter-propagation exceeds advection for all phase shifts in which
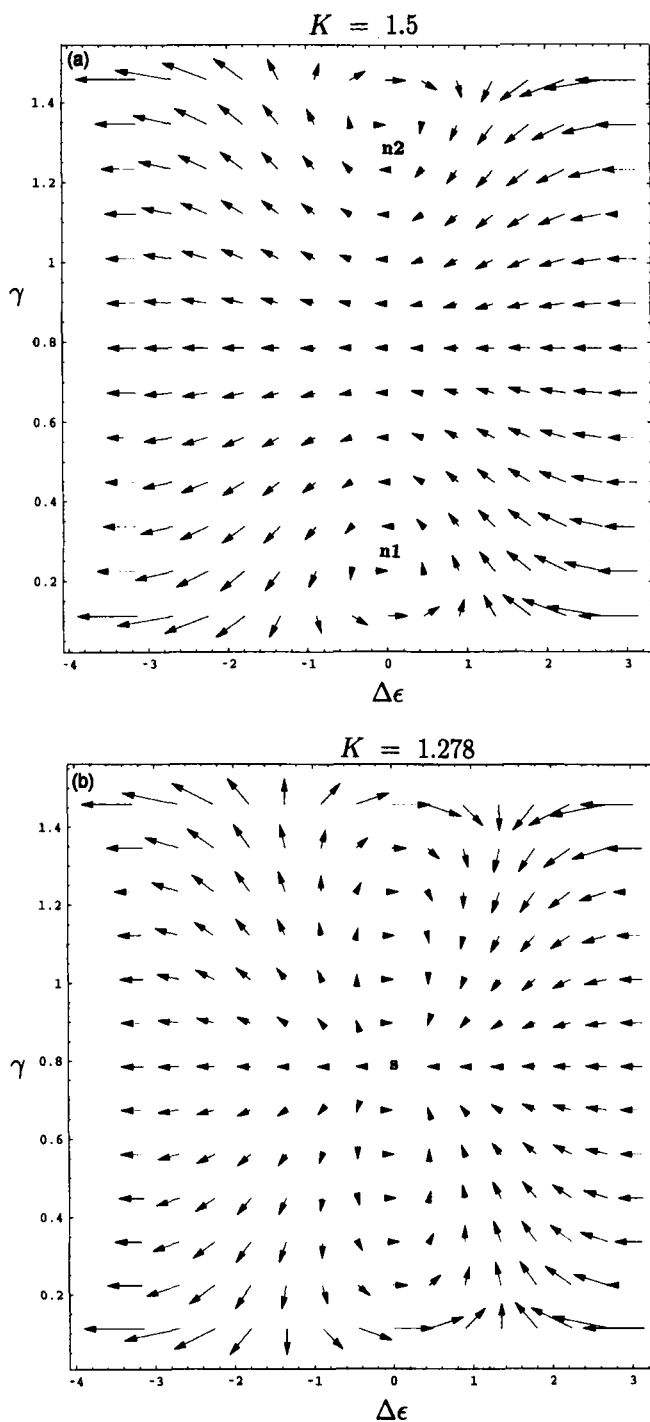
$$K = 1.5$$

$$K = 1.278$$

Figure 3. Phase diagrams for the evolution of the structures of counter-propagating Rossby waves (CRWs) for different wave numbers K. The abscissa is $\Delta\epsilon$, the phase difference between the northern and the southern CRWs; the ordinate is γ, the inverse tangent of the amplitude ratio of the northern and the southern CRWs. The arrows indicate vectors where their x and y components are the time derivatives of $\Delta\epsilon$ and γ respectively, as determined by Eqs. 9(a,b). (a) $K = 1.5$; the two neutral NMs are indicated by 'n1' and 'n2'. (b) $K = 1.278$; the single NM of the short-wave cut-off is indicated by 's'. (c) $K = 1.25$; (d) $K = 1.0$; and (e) $K = 0.797$. The growing and decaying NMs are indicated by 'g' and 'd' respectively in (c), (d) and (e).

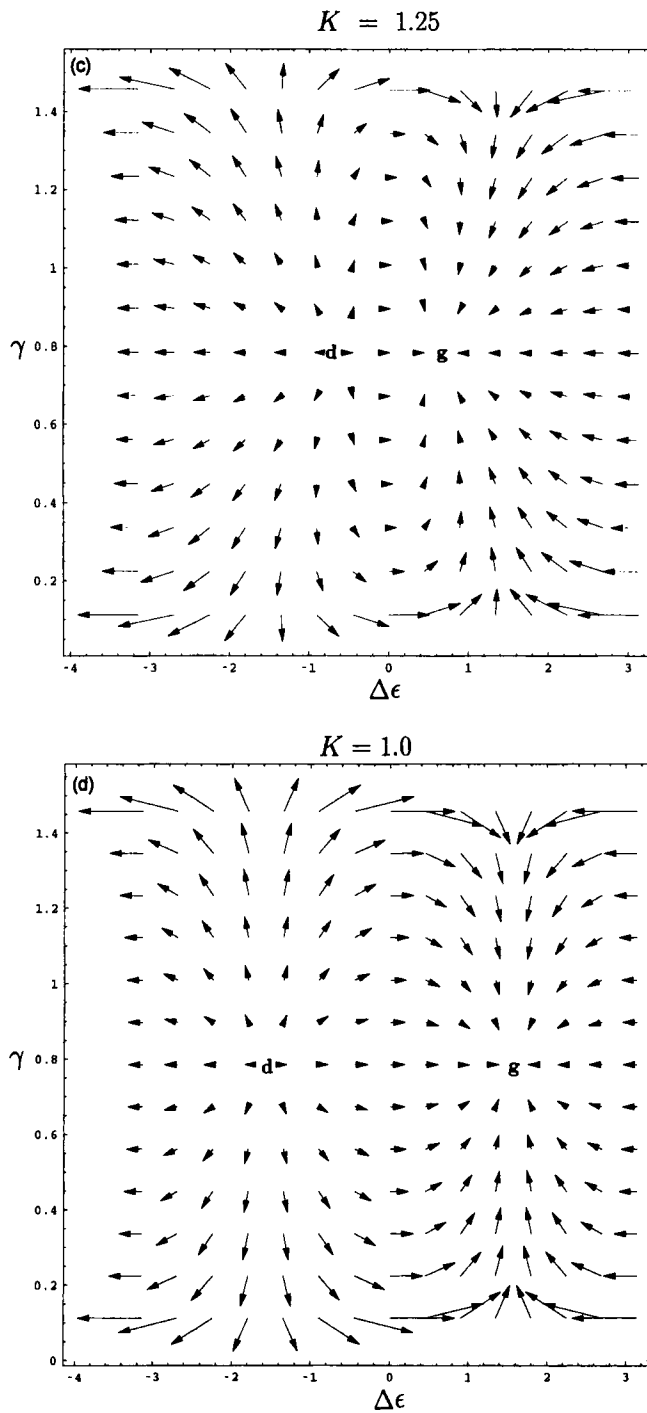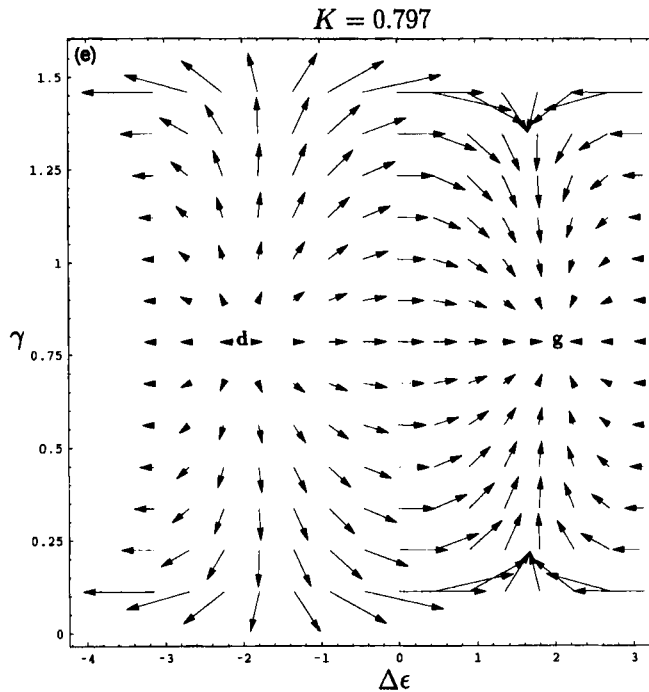$$K = 1.25$$

$$K = 1.0$$

Figure 3.   Continued.

$$K = 0.797$$

Figure 3.   Continued.

$|\Delta\epsilon| < \pi/2$, while advection exceeds counter-propagation whenever $|\Delta\epsilon| > \pi/2$. Note that (15b) shows that this is true for all wavelengths.

Despite the fact that the structures with γ values near $\pi/4$ will never attain a time invariant structure, growth occurs whenever $\Delta\epsilon > 0$. It is this sort of growth that was discussed by Rotunno and Fantini (1989).

At the critical wavelength $K_c = 1.278$, the single NM at $(\Delta\epsilon, \gamma) = (0, \pi/4)$, is a saddle node (indicated by 's'). For a smaller wave number $K = 1.25$, we see that the $\Delta\epsilon$ values of structures can increase for all amplitude ratios provided that the absolute value of $\Delta\epsilon$ is not greater than $\Delta\epsilon_{normal\ mode} = 0.51$. At this wavelength, counter-propagation can dominate advection at all amplitude ratios provided that the northern and southern waves sufficiently reinforce each other's wind fields. The structural invariance of the stable and unstable nodes on this phase diagram means that they respectively correspond to the growing and decaying NMs (indicated by 'g' and 'd'). In these NM structures, counter-propagation is exactly balanced by mean flow advection. Note that, apart from the decaying NM, all modes gradually attain the stable structure of the amplifying NM.

For $K = 1$, the structure is similar to the $K = 1.25$ figure, except that here the NMs have a phase shift of a quarter of a wavelength, cf. Fig. 4. As should be clear from our earlier discussion of isolated edge waves, at this wavelength the edge waves do not need assistance to offset advection by the mean flow.

Interestingly, although the $K = 1$ NM has a quarter of a wavelength phase shift, which according to (14a) and (14b) is an optimal phase shift for growth, the $K = 1$ is not the most rapidly growing normal mode. Why?

It is the wind field attributable to the vorticity of the opposed CRW that causes each CRW to grow. The strength of this attributable wind field depends on the meridional scale of the wave. HMR refer to this dependency as the scale effect. For the Rayleigh
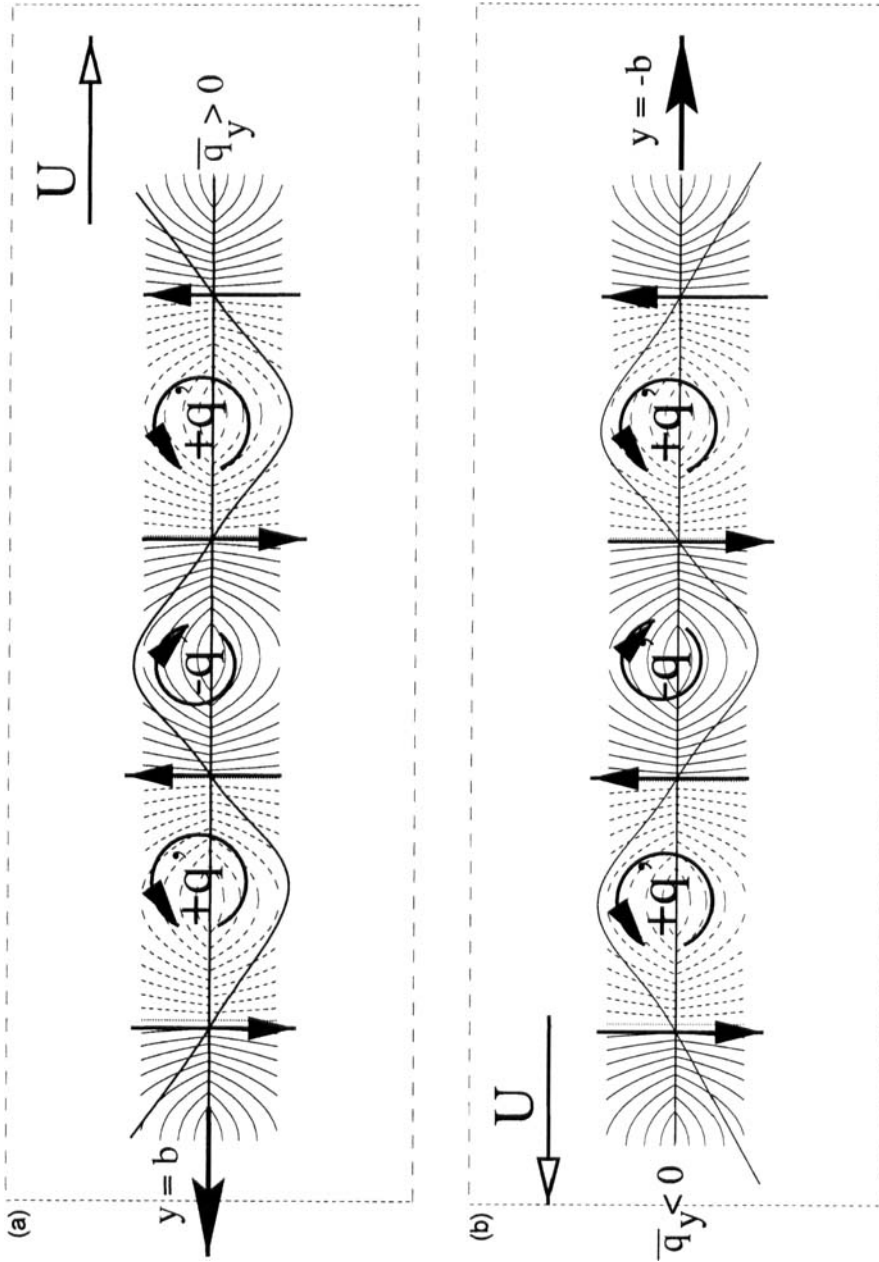
Figure 4. The interaction between the two CRWs, illustrated in Figs. 2(a) and (b), corresponding to wave number $K = 1$ growing NM. The CRWs are a quarter of a wavelength out of phase. The dashed arrows indicate the wind induced by each CRW on the opposing CRW (attenuated by e^{-K}). Since the induced wind is correlated with the meridional displacement of the opposing CRW it makes the latter grow.

problem, the wind attributable to the vorticity CRW at one edge is attenuated by a factor
of e^{-K} by the time it reaches the opposing edge. Thus, there is a trade-off between
the optimal phase for mutual amplification ($\Delta\epsilon = \pi/4$) and the wavelength for minimal
attenuation ($K = 0$), since both of these properties are functions of the wavelength. The
maximal growth rate:

$$\frac{\partial}{\partial K}(K C_{inm}) = \frac{1}{2}\left\{\sin(\Delta\epsilon)\frac{\partial}{\partial K}(e^{-K}) + e^{-K}\frac{\partial}{\partial K}\sin(\Delta\epsilon)\right\} = 0, \qquad (16)$$

is obtained for the wave number $K_{max} \approx 0.797$ and the phase difference $\Delta\epsilon_{max} \approx$
0.646π, see Figs. 1(b) and 3(e). The phase diagram for non-modal waves at the wave
number is given in Fig. 3(d).

The CRWs approach is not limited only to two interacting Rossby waves, and in
fact CRWs can be generated on every interface that lies between two different vorticity
strips. Also, since any mean wind profile, $\overline{U}(y)$, can be approximated, in principle,
by a piecewise–linear function, such an approximation breaks apart the mean flow
into sequences of different vorticity strips. Then, the perturbation dynamics can be
crudely represented in terms of the *multi*-interactions between all of the CRWs that
are generated on the interfaces between each pair of neighbouring vorticity strips. In
order to demonstrate such a process, we discuss in the following section, a simple *multi*-
interaction between three CRWs.

3. Two Vorticity strips

Consider the basic state (Fig. 5(a)):

$$\overline{U} = \begin{cases} 0 & \text{for } y \geqslant b \\ \Lambda(b-y) & \text{for } 0 \leqslant y < b \\ \Lambda(b+y) & \text{for } -b \leqslant y < 0 \\ 0 & \text{for } y \leqslant -b \end{cases} \quad \text{and} \quad \overline{q} = \begin{cases} 0 & \text{for } y \geqslant b \\ \Lambda & \text{for } 0 \leqslant y < b \\ -\Lambda & \text{for } -b \leqslant y < 0 \\ 0 & \text{for } y \leqslant -b. \end{cases} \qquad (17)$$

This flow crudely resembles a barotropic jet, or if we add a constant mean wind
$\overline{U} = -\Lambda b$, it may be viewed as a rough approximation to the leeward wake of westward
flow around isolated topography, e.g. Schär and Smith (1993).

The discrete spectrum solution can be represented by three CRWs, which are located
on the three mean vorticity interfaces $y = \{-b, 0, b\}$, with the stream function:

$$\psi' = \{S(t)\,e^{-k|y+b|}\,e^{i\epsilon_s(t)} + M(t)\,e^{-k|y|}\,e^{i\epsilon_m(t)} + N(t)\,e^{-k|y-b|}\,e^{i\epsilon_n(t)}\}\,e^{ikx}, \qquad (18)$$

where S, M and N are the amplitudes of the southern, middle and northern CRWs
respectively, and ϵ_s, ϵ_m and ϵ_n are their phases. Substituting (18) into (2) for the three
interfaces, gives the equations governing the CRWs, viz:

$$\frac{1}{S}\frac{\partial S}{\partial t} = \frac{\Lambda}{2}\left\{-e^{-K/2}\left(\frac{M}{S}\right)\sin(\epsilon_s - \epsilon_m) - e^{-K}\left(\frac{N}{S}\right)\sin(\epsilon_s - \epsilon_n)\right\}, \qquad (19a)$$

$$\frac{1}{M}\frac{\partial M}{\partial t} = \Lambda\left\{e^{-K/2}\left(\frac{N}{M}\right)\sin(\epsilon_m - \epsilon_n) + e^{-K/2}\left(\frac{S}{M}\right)\sin(\epsilon_m - \epsilon_s)\right\}, \qquad (19b)$$

$$\frac{1}{N}\frac{\partial N}{\partial t} = \frac{\Lambda}{2}\left\{-e^{-K/2}\left(\frac{M}{N}\right)\sin(\epsilon_n - \epsilon_m) - e^{-K}\left(\frac{S}{N}\right)\sin(\epsilon_n - \epsilon_s)\right\}, \qquad (19c)$$

$$c_s = -\frac{1}{k}\frac{\partial \epsilon_s}{\partial t} = \frac{\Lambda b}{K}\left\{1 + \left(e^{-K/2}\frac{M}{S}\right)\cos(\epsilon_s - \epsilon_m) + \left(e^{-K}\frac{N}{S}\right)\cos(\epsilon_s - \epsilon_n)\right\},$$

(19d)

$$c_m = -\frac{1}{k}\frac{\partial \epsilon_m}{\partial t} = \Lambda b\left[1 - \frac{2}{K}\left\{1 + \left(e^{-K/2}\frac{N}{M}\right)\cos(\epsilon_m - \epsilon_n)\right. \right.$$
$$\left. \left. + \left(e^{-K/2}\frac{S}{M}\right)\cos(\epsilon_m - \epsilon_s)\right\}\right],$$

(19e)

$$c_n = -\frac{1}{k}\frac{\partial \epsilon_n}{\partial t} = \frac{\Lambda b}{K}\left\{1 + \left(e^{-K/2}\frac{M}{N}\right)\cos(\epsilon_n - \epsilon_m) + \left(e^{-K}\frac{S}{N}\right)\cos(\epsilon_n - \epsilon_s)\right\}.$$

(19f)

The above equations describe similar interactions to those described by (14). Here, however, the growth and the counter-propagation of each CRW is affected by the meridional wind attributable to not one but to two other CRWs.

Looking for the symmetric NMs solution where $\frac{1}{S}\frac{\partial S}{\partial t} = \frac{1}{M}\frac{\partial M}{\partial t} = \frac{1}{N}\frac{\partial N}{\partial t} \equiv kc_{inm} \neq 0$, then we get from (19a) and (19c) that $\epsilon_s = \epsilon_n$; $M/2 = S = N$; and $kc_{inm} = \Lambda\,e^{-K/2}$ $\sin(\Delta\epsilon_{nm})$, where $\Delta\epsilon_{nm} \equiv \epsilon_m - \epsilon_s = \epsilon_m - \epsilon_n$. Consequently, (19a) and (19c) are effectively equivalent to each other and so (19d) is equivalent to (19f). Thus, the symmetric solution is governed by four equations that have some similarities with the vorticity strip of Rayleigh. The same real phase-speed condition, $c_s = c_n \equiv c_{rnm}$, requires from (19d) to (19f) that

$$\Delta\epsilon_{nm} = \pm\cos^{-1}[-\{e^{K/2}(3 - K) + e^{-K/2}\}/4],$$

(20)

where positive $\Delta\epsilon$ refers to the growing mode. Note that in this problem the modes are not stationary but propagate with a phase speed:

$$c_{rnm} = \frac{\Lambda b}{2K}(e^{-K} + K - 1),$$

(21)

which decreases with the wavelength.

As in the original Rayleigh problem as $K \to 0$, then $\Delta\epsilon_{nm} \to \pi$. According to (20) also, the middle CRW is $\pi/2$ upstream of its neighbouring CRWs, i.e. in a pure configuration for amplification, when $K = 3 + e^{-K} \approx 3.047$. The most unstable NM is obtained for $K_{max} = 2.452$, with a phase difference $\Delta\epsilon_{nm} = 0.682\pi$ and with a growth rate of $\approx 24.7\%$ of the shear Λ. The short wave number cutoff occurs at $K_c = e^{-K_c} + 4\,e^{-K_c/2} + 3 \approx 3.665$. At higher wave numbers all the modes have the same phase, i.e. $\epsilon_m = \epsilon_n = \epsilon_s$ and thus the modes are neutral. Denoting $\chi \equiv M/N$, where $N = S$, the condition $c_s = c_m = c_n = c_{rnm}$, yields the quadratic equation $\chi^2 + \{e^{K/2}(3 - K) + e^{-K/2}\}\chi + 4 = 0$. The first root, χ_1, is always larger than 2 for wave numbers larger than the short-wave cut-off. This is the case where the middle CRW is strongly helping the northern and the southern CRWs to counter-propagate to the east and consequently $\Lambda b/2 < c_{rnm} < \Lambda b$. The second root, χ_2, is always between 2 and 0 for these wave numbers, and corresponds to the case where the northern and the southern CRWs are strongly helping the middle CRW to counter-propagate to the west. Consequently, the NM phase speed remains eastward but relatively small, i.e. $0 < c_{rnm} < \Lambda b/2$. The dispersion relation is summarized in Fig. 5(b). The most unstable NM stream function and the three CRWs which compose it, are presented in Fig. 5(c).
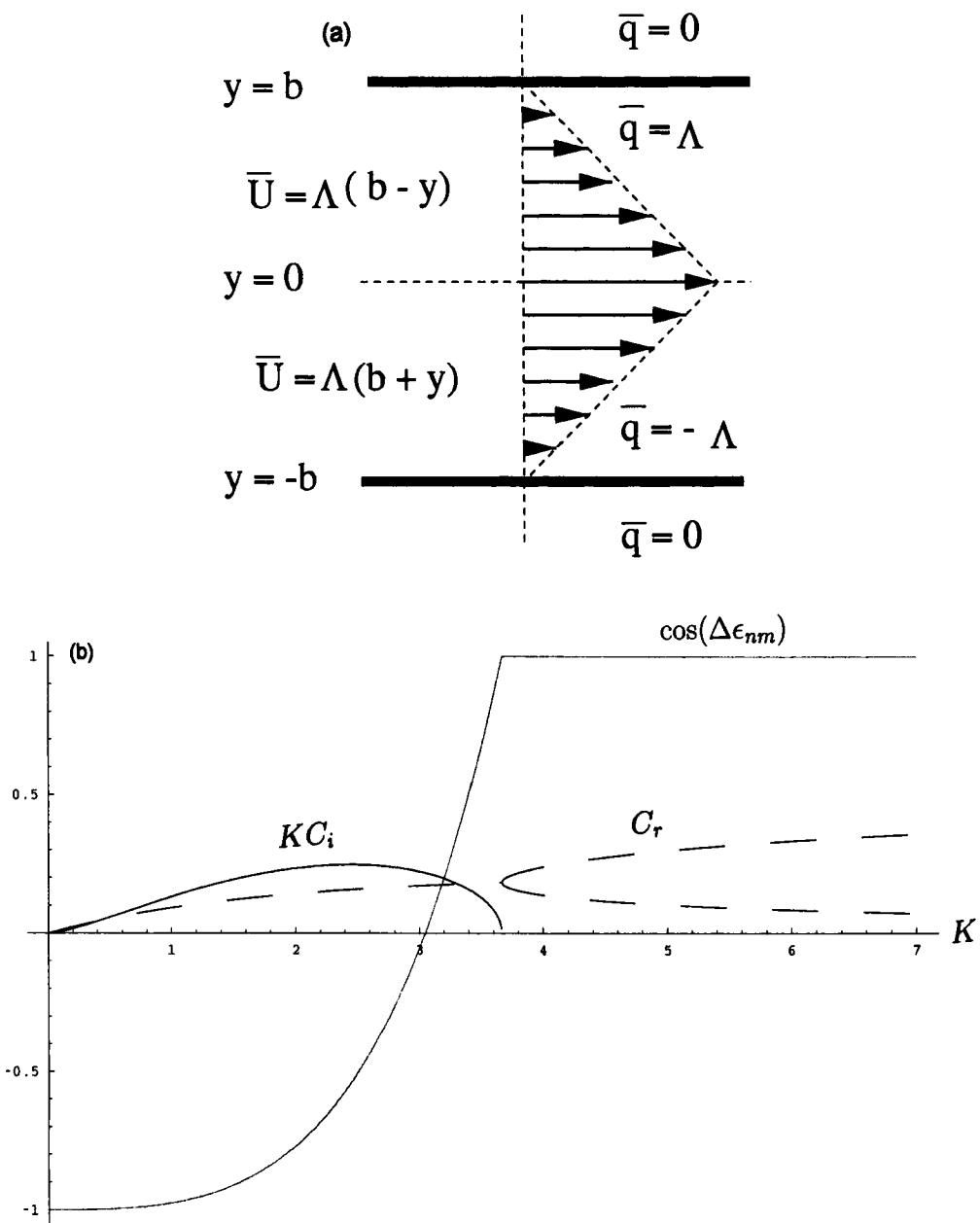
E. HEIFETZ, C. H. BISHOP and P. ALPERT

(a)

$\overline{q} = 0$

$y = b$

$\overline{q} = \Lambda$

$\overline{U} = \Lambda (b - y)$

$y = 0$

$\overline{U} = \Lambda (b + y)$

$\overline{q} = -\Lambda$

$y = -b$

$\overline{q} = 0$

(b)

$\cos(\Delta \epsilon_{nm})$

KC_i

C_r

K

Figure 5.   (a) The barotropic jet. Arrows indicate the zonal mean wind $\overline{U}$; the symbols are as in Fig. 1(a). (b) As Fig. 1(b) but for the dispersion relation of the normal modes, NMs, obtained from the basic state described in Fig. 5(a). Here $\Delta \epsilon_{nm}$ is the phase difference between the counter-propagating Rossby wave (CRW) in the middle and the two CRWs on the edges. (c) Stream function fields of the most unstable NM and the three CRWs that compose it, corresponding to maximum wave number $K_{max} \approx 2.45$. Light shading indicates positive and dark shading negative values.
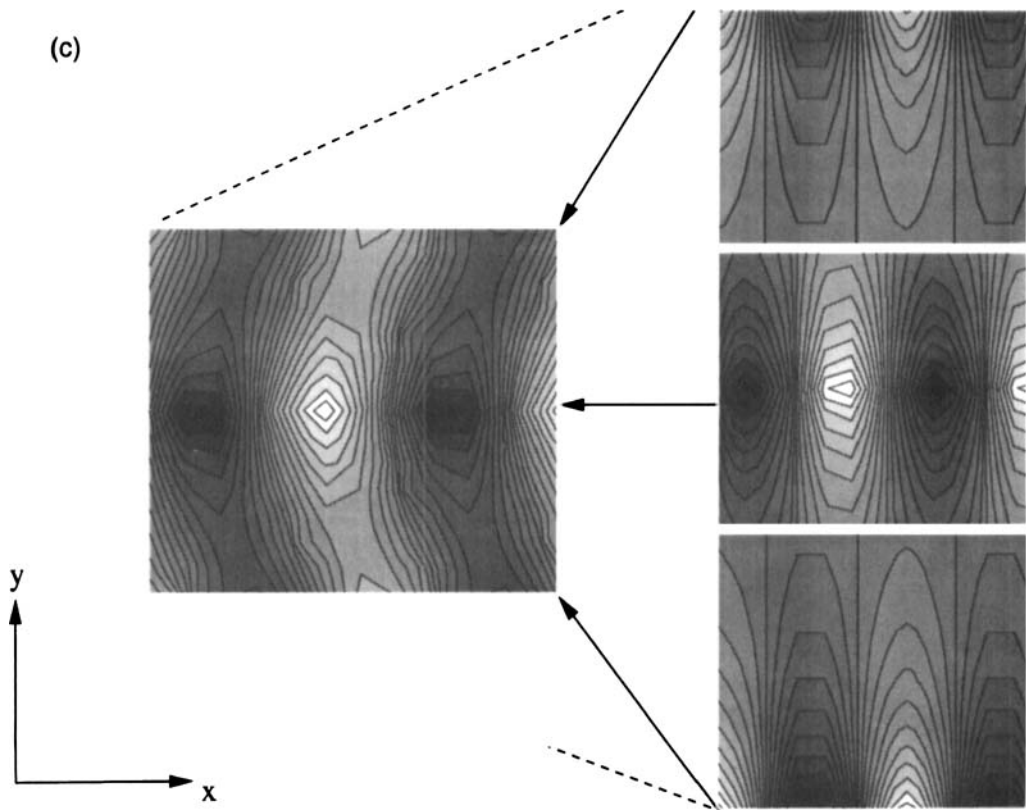
Figure 5. Continued.

4. CONCLUDING REMARKS

The main goal of this paper was to fill a gap in the' present literature on CRWs, which either gives primarily a descriptive picture of the CRW interaction (HMR, for instance) or presents a relatively complicated and detailed rigorous analysis (Davies and Bishop 1994, for instance). Here, we have presented one of the simplest problems that the CRW approach can be applied to—the Rayleigh (1880) problem. Because of the simple inversion relation between vorticity and stream function, the roles of the different terms in the CRWs' dynamic equation are relatively easy to interpret.

We have argued that the 'explanation' of shear flow instability that can be gleaned from standard NM analyses is unsatisfactory as it does not provide tools to make qualitative estimates of how non-trivial changes in the basic state shear flow will affect the stability of the shear flow. Furthermore, it does not provide an overview of how the structure of all possible linear combinations of conjugate NMs will evolve in time. In contrast, the CRW perspective makes it very easy to predict how the complete range of modal and non-modal waves will evolve. It also allows thought experiments to be performed to determine qualitatively how changes in the basic state shear flow are likely to affect the instability of the shear flow.

To illustrate that the CRW approach is not limited to flows with just two distinct PV gradients, we also analysed the stability of a jet flow consisting of two contiguous strips

of oppositely signed vorticity in terms of the interaction of three CRWs, that interact in a similar manner to the two CRWs of the Rayleigh problem.

The two simple models considered in this paper bear a crude resemblance to the shear flows existing at fronts, jets, wake flow beyond topographic obstacles and other meteorological phenomena. While our solutions are far too simple to yield quantitatively reliable information about these flows, the CRW framework should provide qualitatively correct predictions about wave development on these flows.

REFERENCES

Barcilon, A. and Bishop, C. H.	1998	Non-modal development of baroclinic waves undergoing horizontal shear deformation. *J. Atmos. Sci.*, **55**, 3583–3596
Bishop, C. H.	1993a	On the behaviour of baroclinic waves undergoing horizontal deformation. I: The 'RT' phase diagram. *Q. J. R. Meteorol. Soc.*, **119**, 221–240
	1993b	On the behaviour of baroclinic waves undergoing horizontal deformation. II: Error bound amplification and Rossby wave diagnostics. *Q. J. R. Meteorol. Soc.*, **119**, 241–267
Bishop, C. H. and Heifetz, E.	1999	Absolute instability and the continuous spectrum. *J. Atmos. Sci.*, in press
Bishop, C. H. and Thorpe, A. J.	1994	Frontal wave stability during moist deformation frontogenesis. Part I: Linear wave dynamics. *J. Atmos. Sci.*, **51**, 852–873
Bretherton, F. P.	1966	Baroclinic instability and the short wave cut-off in terms of potential vorticity. *Q. J. R. Meteorol. Soc.*, **92**, 335–345
Case, K. M.	1960a	Stability of inviscid plane Couette flow. *Phys. Fluids*, **3**, 143–148
	1960b	Stability of an idealized atmosphere. I. Discussion of results. *Phys. Fluids*, **3**, 149–154
Charney, J. G.	1947	The dynamics of long waves in a baroclinic westerly current. *J. Meteorol.*, **4**, 135–163
Charney, J. G. and Stern, M. E.	1962	On the stability of an internal baroclinic jet in a rotating atmosphere. *J. Atmos. Sci.*, **19**, 159–172
Davies, H. C. and Bishop, C. H.	1994	Eady edge waves and rapid development. *J. Atmos. Sci.*, **51**, 1930–1946
Drazin, P. G. and Howard, L. N.	1966	Hydrodynamic stability of parallel flow of inviscid fluid. *Adv. Appl. Mech.*, **7**, 1–89
Dritschel, D. G.	1989	On the stabilization of a two-dimensional vortex strip by adverse shear. *J. Fluid. Mech.*, **206**, 193–221
Dritschel, D. G., Haynes, P. H., Juckes, M. N., McIntyre, M. E. and Shepherd, T. G.	1991	The stability of a two-dimensional vorticity filament under uniform strain. *J. Fluid. Mech.*, **230**, 647–665
Eady, E. T.	1949	Long waves and cyclone waves. *Tellus*, **1**, 33–52
Eliassen, A., Höiland, E. and Riis, E.	1953	Two-dimensional perturbations of a flow with constant shear of a stratified fluid. *Weather Climate Res.*, **1**, 149–150
Farrell, B. F.	1984	Modal and non-modal baroclinic waves. *J. Atmos. Sci.*, **41**, 668–673
	1988	Optimal excitation on neutral Rossby waves. *J. Atmos. Sci.*, **45**, 1663–1686
Gaster, M.	1962	A note on the relation between temporally increasing and spatially increasing disturbances in hydrodynamic stability. *J. Fluid. Mech.*, **14**, 222–224
Gill, A. E.	1982	*Atmosphere–ocean dynamics*. Academic Press, New York, USA
Heifetz, E.	1999	'Understanding Baroclinic Instability by using the 'Lagrangian Parcel Method' and the 'Counter-propagating Rossby Waves approach'. Doctoral Dissertation, Tel-Aviv University

Holton, J. R.   1992   *An introduction to dynamical meteorology.* 3rd Edition, Academic
                                                         Press, New York, USA

Hoskins, B. J., McIntyre, M. E. and   1985   On the use and significance of isentropic potential vorticity maps.
    Robinson, W.   *Q. J. R. Meteorol. Soc.,* **111,** 877–946

Pedlosky, J.   1964   An initial-value problem in the theory of baroclinic instability.
                                                         Tellus, **16,** 12–17

Rayleigh, Lord.   1880   On the stability, or instability, of certain fluid motions. *Proc.*
                                                         London Math. Soc., **9,** 57–70

Rotunno, R. and Fantini, M.   1989   Pettersen's 'Type B' cyclogenesis in terms of discrete, neutral
                                                         Eady modes. *J. Atmos. Sci.,* **51,** 3559–3604

Schär, C. and Smith, R. B.   1993   Shallow-water flow past isolated topography. Part I: Vorticity
                                                         production and wake formation. *J. Atmos. Sci.,* **50,** 1373–
                                                         1400

Watson, M.   1962   On spatially growing finite disturbances in plane Poiseuille flow.
                                                         J. Fluid. Mech., **14,** 211–221